Received: 28 February 2021 | Revised: 17 May 2021 | Accepted: 28 May 2021

IET Microwaves, Antennas & Propagation

DOI: 10.1049/mia2.12166

The Institution of Engineering and Technology WILEY

ORIGINAL RESEARCH PAPER

Complex eigenvalues of natural *TM*-oscillations in an open resonator formed by two sinusoidally corrugated metallic strips

Elena D. Vinogradova[1] | **Kazuya Kobayashi**[2]

[1]Department of Mathematics and Statistics, Macquarie University, Sydney, Australia

[2]Department of Electrical, Electronic, and Communication Engineering, Chuo University, Hachioji, Japan

Correspondence

Elena Vinogradova, Department of Mathematics and Statistics, Macquarie University, NSW2109, Sydney, Australia.
Email: elena.vynogradova@mq.edu.au

Abstract

The diffraction of an E-polarized plane wave from two finite sinusoidal gratings is investigated by a rigorous approach, based on the Method of Analytical Regularization. This allows us to analyse the problem in a wide frequency band without limitations on the depth of the sinusoidal corrugation, the wave size of the gratings, or their relative location. The homogeneous version of the equations obtained is used for accurate computation of the complex eigenvalues in an open resonator of Fabry–Perot type with sinusoidally corrugated strips. In the calculations, two types of structures were used: one is formed by parallel translation of the sinusoidally corrugated strips and the other is obtained by rotation of one of the strips in the first structure. For each relative location of the corrugated strips, the resonance excitation of the structure by an obliquely incident E-polarized plane wave is considered. Based on the calculation of the surface current density for different incidence angles, their specific values for optimal excitation of the complex modes are established.

1 | INTRODUCTION

The theoretical foundation for the analysis of periodic structures has developed over many years with various approaches. As mentioned in [1], the variety of existing methods is due not just to historical reasons but mainly to the absence of a universal approach for solving all diffraction problems related to periodic structures. The great number of existing methods is explained by the complexity and variety of the structures and their applications. There are a vast number of surveys, monographs and handbooks (see e.g. [1–4]) which comprehensively describe both the physical phenomena, arising under excitation of periodic structures by acoustic and electromagnetic radiation, and the methods of their analysis. In general, applications where use of periodic structures is of paramount significance cover diverse aspects of theoretical and technical physics. One example is the theory of beam-plasma instability in a periodic plasma-filled waveguide [5], where a planar symmetrical metallic waveguide with arbitrary periodic walls is considered as a basic element. Modelling the effect of plasma on the diffraction radiation of a relativistic beam moving over a grating of finite extent is highlighted in [6]. It should be noticed, in [5, 6], that the authors treated the electromagnetic part of both problems in a rigorous fashion, applying the idea of analytical regularization to surface integral equations.

Among the different aspects which concern analysis of periodic structures, one is of special interest: the transition from infinite periodic structures to their truncated (finite) versions. In practice, only finite structures are employed whilst the overwhelming majority of research is devoted to analysis of infinite structures. This circumstance raises questions about applicability of the theory developed for infinite gratings to their finite counterparts. Foremost, which parameters of the finite grating should be chosen to provide the most important property of diffraction grating, the creation of diffraction orders (or Floquet harmonics)? An adequate theory describing finite periodic structures should be able to evaluate the impact of the truncation of an infinite structure to a finite number of periods and of the corresponding *end effects* on the emerging Floquet harmonics (or diffraction orders) described by the *grating formula*. It should be noticed that almost all investigations on finite gratings have been performed for planar strip or slit gratings.

The article [7] is one of the earliest analyses of a two PEC-strip open resonator that employed the MAR: it employed inversion of the static-part in the Fourier-transform domain. In [8, 9], the authors used the so-called *operator method* to investigate electromagnetic wave diffraction by planar screens (strips) and diffraction of an H-polarized plane wave by a finite layered graphene strip grating, respectively. In the construction of the solution, the key role is played by the scattering operators of a single-layer potential, finally reducing both problems to a set of integral equations. The diffraction of Hermite–Gaussian beams by N equally spaced slits in a planar screen (a lamellar finite grating) at the scalar diffraction regime is analysed in [10, 11]. Further studies of planar finite gratings may be found in [12–14]. In [13], the authors used a highly pragmatic approach and compared numerical results for induced surface current density on the strips in finite and infinite gratings, logically assuming that with each increase of the number of strips, the induced current on each strip will be approaching that of the strips in the infinite grating (see also [15]).

Turning to the concrete content of the present article, our investigation focuses on perfectly conducting surface-relief gratings with sinusoidal corrugation. For a long time, plane wave diffraction problems for both E- and H-polarization for finite sinusoidal single gratings [16] and binary gratings [17] have been analysed by the Wiener–Hopf technique combined with a perturbation method. In these articles, the initial stage of the solution assumes that the depth of the grating is small compared with the wavelength. In addition, this technique is only applicable for analysis of diffraction in the far-field zone and fails when the plane wave strikes the grating surface at a grazing angle. In a recently published article [15], we compared results of finite sinusoidal gratings obtained by the Wiener–Hopf technique combined with a perturbation method and those obtained by the rigorous Method of Analytical Regularization (*MAR*). The accuracy of the rigorous *MAR* in the specific case of sinusoidally corrugated gratings was accurately established in Sections 2.2 and 4.1 of the article [15]; it allowed us to treat the *MAR* as an instrument for assessing the accuracy of the approximations in the other solutions obtained by the rigorous Wiener–Hopf technique combined with the perturbation method. It was shown that the replacement of the exact boundary conditions by impedance-type boundary conditions when the depth ($2h$) of the grating is small compared with the wavelength (not exceeding the 'threshold' value $2h/\lambda \leq 0.1$) is justified: comparison with accurate *MAR* results reveals excellent coincidence. In general, the *MAR* allowed us, for the first time, to investigate the problem without restrictions that are usually imposed on the depth of the grating, the number of the periods and the frequency range. In addition, the *MAR* provides the calculation of the diffracted waves in both the near- and far-field zones. This property is used in the present article, focusing mostly on the calculation of resonance surface current density arising as a result of excitation of standing TM-modes. The main result of our investigation is an accurate calculation of the complex eigenvalues of natural oscillations in a parallel-strip open resonator with transversely corrugated strips. In principle, the *MAR* approach for open resonators with corrugated strips allows the corrugation to be described by any given arbitrary smooth contour. In this article, we deal with sinusoidal corrugation. To the best of our knowledge, this is the first time that such an investigation has been undertaken, at least in a rigorous fashion, in which the computation of the complex eigenvalues is accompanied by an assessment of their accuracy.

The methodology of studies of the spectrum, based on the *MAR,* is treated in detail in [18], where the spectrum of the complex eigenvalues for a sound-soft slotted elliptical cavity is comprehensively investigated. The article is organized as follows: In the next section, we briefly describe the theoretical aspects, explaining the core of the *MAR*-based rigorous approach (Section 2.1), and then employ it for analysis of the spectrum (Section 2.2). From the variety of permissible locations of two strips, transversely corrugated in a sinusoidal manner, we consider, in Sections 3.1 and 3.2, two types of parallel-strip resonators The first type, which we call 'anti-symmetric', is shown in Figure 1a, where the upper strip is a translation of the lower corrugated strip in a direction parallel to the y-axis (see Section 3.1). The second type, which we call 'symmetric' may be obtained from the first by rotation of the upper strip by 180° (see Figure 1b). In Section 3.3, we use the results of the spectrum of complex relative wave numbers, obtained in the previous Sections 3.1 and 3.2, for calculation of the resonance surface current density induced by an E-polarized plane wave. In Section 4, we examine the problems related to resonance scattering of an obliquely incident E-polarized plane wave by a parallel-strip resonator with sinusoidally corrugated walls. In Section 5, we outline the results obtained and describe further investigations which may be performed with the use of the *MAR*.

2 | THEORETICAL ASPECTS OF THE PROBLEM

2.1 | Schematic description of the solution procedure applying the *MAR*

The results are based on the mathematically correct solution of the mixed boundary value problem for the Helmholtz equation with Dirichlet's boundary conditions imposed on the corrugated strips. This problem arises during illumination of the strips by an obliquely incident E-polarized plane wave. The statement of the problem is free from restrictions which may be imposed on the number of finite sinusoidal gratings as well as on their relative location; however, in this article, we use only one of the possibilities, substituting the planar strips in a parallel-strip resonator of Fabry–Perot type by sinusoidally corrugated strips. The problem geometry is shown in Figure 1. The relative locations of the sinusoidally corrugated *PEC* strips are defined by their symmetry relative to the plane $X0Y$. It should be noticed that the apparently excessively deep scale of the corrugation shown in Figure 1 is only for a clear description of the geometry.

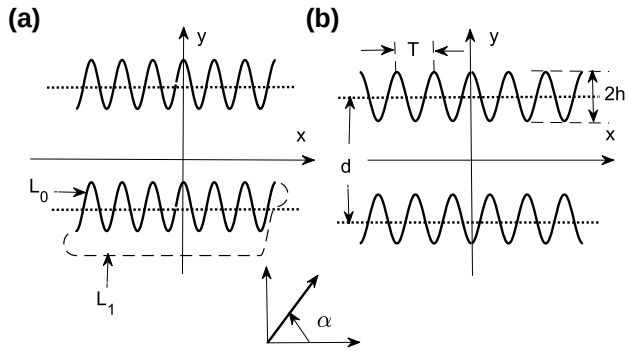

FIGURE 1 Excitation of the parallel-strip resonator with sinusoidally corrugated strips by an obliquely incident plane wave: (a) 'anti-symmetric' arrangement; (b) 'symmetric' arrangement

The parallel-strip resonator with corrugated strips is described by four geometrical parameters: (a) d, the distance between the strips; (b) h, the amplitude of corrugation; (c) T, the period of sinusoidal corrugation; and (d) n_T, the number of the periods placed along each strip. With the choice of axes shown in Figure 1, an E-polarized plane wave incident on the open resonator has the form $E_z^0 = e^{ik(x\cos\alpha + y\sin\alpha)}e^{-i\omega t}$; it is characterized by the incident angle α and the wave number $k = 2\pi/\lambda$. The time harmonic dependence $e^{-i\omega t}$ is suppressed throughout the article.

The problem to be solved does not possess any special features which would otherwise require a modification of the standard *MAR* for the concrete geometry of the problem; it is a mild variation of the '*2-D open cavity problem*' solved by the *MAR* in [19]. Instead of the single open cavity, studied in [19], we consider the upper and lower strips of the open resonator as two interacting 'cavities'; from the theoretical point of view, the main steps of the *MAR* solution procedure are essentially the same.

Let us explain by considering first the lower corrugated strip of the resonator as an isolated scatterer. In solving this problem in [15], we arrived at an infinite system of coupled linear algebraic equations of the second kind, having the form

$$\begin{aligned}(I + H_{11})X + H_{12}Y &= B_1\\ H_{21}X + (I + H_{22})Y &= B_2\end{aligned}. \tag{1}$$

Here $X = \{X_n\}_{n=0}^{\infty}$ and $Y = \{Y_n\}_{n=1}^{\infty}$ are infinite sets of unknown coefficients, I is the identity operator, H_{ij} $(i,j = 1,2)$ are completely continuous (compact) operators in the functional space of the square summable sequences l_2; and $B_1 \equiv \{B_{1n}\}_{n=0}^{\infty}$ and $B_2 \equiv \{B_{2n}\}_{n=0}^{\infty}$ are the Fourier coefficients of known functions defined by an incident plane wave. The coupling arises between the '*symmetric*' and '*anti-symmetric*' parts of the solution, described by infinite sets of the coefficients $X = \{X_n\}_{n=0}^{\infty}$ and $Y = \{Y_n\}_{n=1}^{\infty}$. This solution describes any isolated corrugated strip of the form pictured in Figure 1. As part of the procedure, the contour L_0 describing the lower corrugated plate in Figure 1b is completed, by the addition of a virtual contour L_1, to form a smooth closed contour $L = L_0 \cup L_1$. (The choice of L_1 is at our disposal—the only requirement is that the closed contour L is smooth.) This preliminary step immediately makes the problem for an isolated corrugated strip solvable by the *MAR* approach which was developed in [19] and is based on the analytical inversion of the static part of the scattering problem with the aid of the Abel transform technique. The Fredholm nature of the operators, H_{ij} $(i,j = 1,2)$ in Equation (1), ensures the fulfilment of the *Fredholm alternative*. It implies the applicability of the truncation method for the numerical solution of the system (1). The *MAR* allows us to achieve not only the convergence itself but also *fast* convergence of the truncated system. One of the merits of the *MAR* is the ease of matrix filling: the matrix elements are combinations of the Fourier coefficients of the smooth part of the integral kernel (rapidly computable by the *Fast Fourier Transform* (*FFT*)) and of the incomplete scalar products of the normalized Jacobi polynomials which, in turn, are very efficiently computed by recurrence relations [20].

Now, consider the scattering problem for the structure depicted in Figure 1. The contour of the upper strip is completed to a closed smooth contour in a similar fashion to that described for the lower plate in the previous paragraph. (As a technical point, the closed contours associated with the upper and lower points must not touch or intersect.) The application of the *MAR* produces a coupled system of linear algebraic equations of the second kind involving four infinite sets of unknown coefficients: $X^{(1)} \equiv \{X_n^{(1)}\}_{n=0}^{\infty}$, $Y^{(1)} \equiv \{Y_n^{(1)}\}_{n=1}^{\infty}$, $X^{(2)} \equiv \{X_n^{(2)}\}_{n=0}^{\infty}$, $Y^{(2)} \equiv \{Y_n^{(2)}\}_{n=1}^{\infty}$. The first pair ($X_n^{(1)}$and $Y_n^{(1)}$) relates to the upper corrugated strip, the second ($X_n^{(2)}$and $Y_n^{(2)}$), to the lower. In operator form, the final system of equations may be represented as follows:

$$\begin{cases}\begin{cases}(I + H_{11}^{(1)})X^{(1)} + H_{12}^{(1)}Y^{(1)} + S_{11}^{(1,2)}X^{(2)} + S_{12}^{(1,2)}Y^{(2)} = B_1^{(1)}\\ H_{21}^{(1)}X^{(1)} + (I + H_{22}^{(1)})Y^{(1)} + S_{21}^{(1,2)}X^{(2)} + S_{22}^{(1,2)}Y^{(2)} = B_2^{(1)}\end{cases}\\ \begin{cases}S_{11}^{(2,1)}X^{(1)} + S_{12}^{(2,1)}Y^{(1)} + (I + H_{22}^{(2)})X^{(2)} + H_{12}^{(2,2)}Y^{(2)} = B_1^{(2)}\\ S_{21}^{(2,1)}X^{(1)} + S_{22}^{(2,1)}Y^{(1)} + H_{21}^{(2,2)}X^{(2)} + (I + H_{22}^{(2)})Y^{(2)} = B_2^{(2)}\end{cases}\end{cases}. \tag{2}$$

Here, the non-zero operators $S_{kp}^{(i,j)}(k,p,i,j = 1,2)$ that are additional to those appearing in Equation (1) describe the coupling between two corrugated strips. Formally, this coupling is expressed through the coupling of the four infinite sets of the Fourier coefficients, $X^{(n)}$, $Y^{(n)}$ $(n = 1,2)$. The upper indexes, i and j, in the notation of the coupling operators $S_{kp}^{(i,j)}$ stand for the numeration of the corrugated strips: the first $(i = 1$ or $j = 1)$ or second $(i = 2$ or $j = 2)$. The meaning of the lower indexes is as follows: The values $k = 1$ or $p = 1$ symbolize the even part of the solution; the values $k = 2$ or $p = 2$, the odd part. For example, the indices of the operator $S_{12}^{(1,2)}$ signify the coupling of the even part of the solution for the first strip with the odd part of the solution for the second strip. The coupling operators $S_{kp}^{(i,j)}$, as

well as the operators H_{ij} $(i,j=1,2)$ are completely continuous (compact) operators in the functional space of the square summable sequences l_2. Such properties ensure the fast convergence of the truncated systems; this is typical for all systems of equations obtained by the *MAR*.

The convergence rate of similar systems has been discussed in many publications (see e.g. [18, 19]). Anticipating that the calculation of the complex eigenvalues (to be discussed in Section 3) requires high accuracy, we illustrate the convergence rate by an example calculation of the relative truncation error e_r as a function of the truncation number for some selected problem parameters. The convergence rate of the truncated systems may be characterized by the *normalized truncation error* $e_r(N_{tr})$, calculated in the maximum norm sense as a function of the truncation number, N_{tr} as

$$e_r(N_{tr}) = \frac{\max_{n \le N_{tr}} \left| Z_n^{N_{tr}+1} - Z_n^{N_{tr}} \right|}{\max_{n \le N_{tr}} \left| Z_n^{N_{tr}+1} \right|}. \tag{3}$$

Here, $Z_n^{N_{tr}}$ and $Z_n^{N_{tr}+1}$ denote the components of the solution $Z = \{X^{(1)} \cup Y^{(1)} \cup X^{(2)} \cup Y^{(2)}\}$ computed with truncation levels N_{tr} and $N_{tr}+1$, respectively; the additional components generated at the truncation level $N_{tr}+1$ are not employed in the calculation (3).

In Figure 2, we plot the typical behaviour of the relative error function, $e_r(N_{tr})$, for systems describing the resonator with strips of symmetric arrangement (Figure 1b) with parameters $n_T = 8$, $T = \lambda/2$, $d = 2\lambda$, and $\alpha = 90^\circ$ and with varying corrugation amplitudes, $h = 0.01\lambda$, 0.05λ, and 0.25λ (see Figure 2a). The value $h = 0$ describes the parallel-strip resonator without corrugation. In Figure 2b, the parameters $n_T = 8$, $T = \lambda/2$, $2L = 4\lambda, h = 0.05\lambda$, and $\alpha = 90^\circ$ are fixed, while the aspect ratio of the distance (d) between equal upper and lower strips and their lengths $(2L)$ varies: $d/2L = 0.5$, 2.5 and 10. The value $d/2L = 0.5$ is usually associated with the parallel-strip waveguide whereas the second $(d/2L = 2.5$ and 10) are usually associated with the Fabry–Perot resonator. The plots $e_r(N_{tr})$ shown in Figure 2 confirm the fast convergence rate of the truncated systems (2) as the truncation number increases. Such convergence will be crucial for the accurate calculation of complex cut-off wave numbers in Section 3.

2.2 | Computation of complex eigenvalues

In this section, we explain the process of computation of the complex eigenvalues of structures when using the *MAR*. The rather straightforward steps for spectral analysis of open 2-D cavities of general shape are provided by the effective solution of the corresponding excitation problem. All these steps are described in detail in [19], where the complex eigenvalues of slotted arbitrary cylindrical cavities are studied, including the sound-soft elliptic cavity with a variably placed longitudinal slit. In the same way, the spectral problem of the structures considered in this article reduces to finding the non-trivial solutions to the homogeneous form of Equation (2). Nulling the right-hand sides in Equation (2), so that $B_1^{(1)} = B_1^{(2)} = B_2^{(1)} = B_2^{(2)} = 0$, we transform the system (2) to a coupled system of homogeneous algebraic equations. It possesses a non-trivial solution if and only if the determinant of these equations equals zero. This

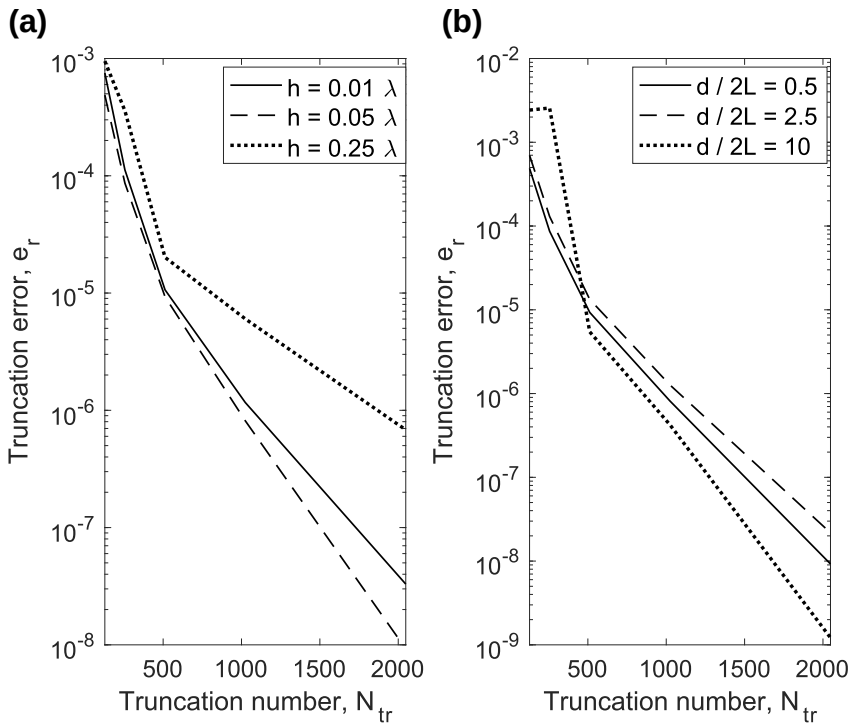

FIGURE 2 Truncation error e_r versus truncation number N_{tr} for corrugated parallel-strip resonator with parameters: (a) $n_T = 8, T = \lambda/2, 2L = 4\lambda, d = 2\lambda, \alpha = 90^\circ$; $h = 0.01\lambda, 0.05\lambda, 0.25\lambda$; (b) $n_T = 8$, $T = \lambda/2$, $2L = 4\lambda, h = 0.05\lambda$, $\alpha = 90^\circ$; $d/2L = 0.5$, 2.5, 10

requirement immediately leads to the characteristic (or dispersion) equation $det(A) = 0$, where A is the matrix of the system of algebraic equations. (Note that the matrix of a second-kind system (2) has a well-defined determinant.) Upon truncation, we solve the equation:

$$det(A_{N_{tr}}) = 0 \tag{4}$$

where $A_{N_{tr}}$ is the appropriately truncated matrix.

For an arbitrary cavity, we face uncertainty in the location of the roots $k_{\text{res}} = k'_{\text{res}} + ik''_{\text{res}}$ of the homogeneous Equation (2) in the complex plane. However, we simply assert that calculation of the spectral dependence of the condition number $cond(A_{N_{tr}})(k)$ for the truncated system immediately provides approximate locations for the real part $Re(k_{\text{res}})$ of the resonance values $k_{\text{res}} = k'_{\text{res}} + ik''_{\text{res}}$. In solving the problem, we employed time-harmonic dependence $e^{-i\omega t}$; hence the imaginary part k''_{res} is always negative ($k''_{\text{res}} < 0$). When the inequality $-k''_{\text{res}} \ll k'_{\text{res}}$ holds, the sharp peaks of the frequency dependence $cond(A_{N_{tr}})(k)$ clearly indicate the location of the values k'_{res} along the real frequency axis k. The accuracy of calculation of the zeros k_{res} of the function $det(A_{N_{tr}})$ strongly depends on the truncation number N_{tr}. By increasing N, one can obtain a prescribed given accuracy of computations.

It should be observed that the term 'spectral parameter' may be variously interpreted. Any parameter (frequency, slit width, or slit position) may play the role of a spectral parameter. In our investigation, we choose the relative wave number kd as the spectral parameter. We explain the algorithm for finding complex eigenvalues by the example of a parallel-strip resonator (without wall corrugation). Calculation of the condition numbers $cond(A_{N_{tr}})(kd)$ of $A_{N_{tr}}$ as a function of the wavenumber kd when $N_{tr} = 128$ (see Figure 3) allows us to find the quasi-singular values kd which correspond to the sharp peaks of this function. Let us fix three resonance values ($kd_{\text{res}_1} = 3.339$, $kd_{\text{res}_2} = 6.410$ and $kd_{\text{res}_3} = 9.518$) and treat them as initial approximations for any standard algorithm for finding the complex-valued roots. Next, we increase the truncation number N_{tr} in order to achieve stabilization at six decimal significant digits in the values of complex cut-off relative wavenumbers.

The stabilization process of the complex eigenvalues, when solving (4) under increasing values N_{tr} , is shown in Table 1, where the bold digits denote the correct digits. The complex relative wavenumbers, $\kappa_n (n = 1, 2, 3)$, are calculated with accuracy of six decimal digits, which is attained when $N_{tr} = 2048$: the values are $\kappa_1 = 3.329760–i0.136971$; $\kappa_2 = 6.409589–i0.056760$; and $\kappa_3 = 9.518394–i0.032476$. An accuracy of four decimal digits is reasonable in practice and is achieved when $N_{tr} = 256$. It is well known that the **unloaded** Q - factor of the complex oscillations is defined by

$$Q_n = -Re(\kappa_n)/(2Im(\kappa_n)),\ n = 1, 2, \ldots \tag{4}$$

In our case, $Q_1 = 12.1549$, $Q_2 = 56.4622$, and $Q_3 = 146.545$. The rather low value of Q_1 explains the noticeable shift of the resonance value $kd_{\text{res}_1} = 3.339$, depicted in Figure 3, from the real part of the cut-off relative wavenumber ($Re(\kappa_1) = 3.329$). When the Q-factor is rather higher, the values kd_{res_i} and κ_i practically coincide: $kd_{\text{res}_3} = 9.518$ and $Re(\kappa_3) = 9.518$, correct to three decimal places.

3 | OPEN PARALLEL CORRUGATED STRIPS RESONATOR

In order to assess the influence of corrugation on the spectrum of the complex eigenvalues, we should first calculate the spectrum of complex eigenvalues for the parallel-strip resonator with non-corrugated strips. To the best of our

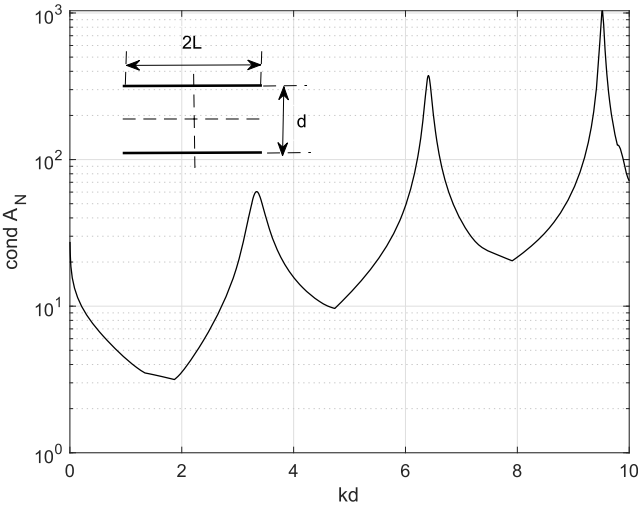

FIGURE 3 Dependence $cond(A_{N_{tr}})(kd)$ for parallel-strip resonator ($d/2L = 0.5$)

TABLE 1 Complex eigenvalues in parallel-strip resonator ($d/2L = 0.5$)

N_{tr}	$kd_{\text{res}_1} = 3.339$	$kd_{\text{res}_2} = 6.410$	$kd_{\text{res}_3} = 9.518$
64	**3.329**687722084370–**i0.13697**1717965096	**6.40**8448538244014–**i0.056**156463605235	**9.51**4325682935294–**i0.032**774151527702
128	**3.3297**47259526723–**i0.13**7009279645877	**6.4095**58713817561–**i0.0567**83888245284	**9.518**216261631725–**i0.0324**80986253740
256	**3.3297**47195572408–**0.13697**8732928400	**6.40958**0194240104–**i0.0567**73945392285	**9.5183**79376759631–**i0.0324**91021576307
512	**3.3297**54917797381–**i0.136971**543906377	**6.40958**4863499405–**I0.05676**2868147102	**9.51839**0858189338–**i0.0324**80741139805
1024	**3.3297**58893367810–**i0.136971**235748391	**6.40958**7670517852–**i0.056760**327824857	**9.51839**3808715686–**i0.03247**7554035563
2048	**3.329760**673337726–**i0.136971**985157022	**6.409589**032347588–**i0.056760**019381560	**9.518394**948530483–**i0.032476**912877430

knowledge, this has not been done previously. Actually, this problem is of independent interest. It was partially considered in the last Section 2.2 where the first three complex oscillations, which may emerge in the parallel planar strips resonator with aspect ratio $d/2L = 0.5$, were studied. It is of interest to examine larger values of kd in order to study further the behaviour of higher complex oscillations and their related complex eigenvalues. The spectral 'portrait' of the waveguide with $d/2L = 0.5$ in the frequency range $10 \le kd \le 50$ is well understood by the dependence $cond(A_{N_{tr}})(kd)$ shown in Figure 4. It can be clearly seen that the advancement to higher frequencies leads to a new phenomenon: the emergence of a train of sub-resonances closely related to the main resonances. To specify these resonances, consider the slightly modified well-known formula for eigenvalues of the *PEC* rectangular box in the form

$$\gamma_{n,m} = k_{nm}d = n\pi\sqrt{1 + \left(\frac{m}{n}\right)^2\left(\frac{d}{2L}\right)^2}, \quad n, m = 1, 2, \ldots \tag{5}$$

where indices n and m stand for the number of electromagnetic field (*EMF*) variations along the length of the resonator and along the transverse direction, respectively. In the limiting case, when $L \to \infty$, one can transform (5) to the well-known formula for parallel-plate waveguide ($\gamma_n = k_n d = n\pi$, $n = 1, 2, \ldots$). The expanded view of $cond(A_{N_{tr}})(kd)$, shown in Figure 4b, allows us to find the correspondence between the results of numerical computation and those obtained by the usage of the formula (5), when we set $d/2L = 0.5$ (see Table 2). Both sequences of results lie close to each other. This observation becomes more pronounced as the parameter $d/2L$ decreases. Comparison of the peak values of the dependence $cond(A_{N_{tr}})(kd)$ with the data calculated by formula (5) when $d/2L = 0.1$ shows a diminished difference in the corresponding values:

$$\gamma'_{14,1} = 43.983(43.980); \qquad \gamma'_{14,2} = 43.986(43.983);$$
$$\gamma'_{14,3} = 43.992(43.988);$$
$$\gamma'_{14,4} = 44.000(43.996) \text{ and } \quad \gamma'_{14,5} = 44.010(44.006).$$

Here, the first value is calculated by (5), and the second (in brackets) is extracted from the graph of the dependence $cond(A_{N_{tr}})(kd)$. This observation signals the emergence of standing waves, even when the rectangular resonator is open. In the case of the parallel-strip resonator, the sharp edges of the strips play the same role as the termination in the rectangular waveguide, creating standing waves between the ends of the parallel-plate waveguide; however, this effect is much weaker than that produced by the *PEC* termination in a rectangular waveguide.

The above arguments and results will be helpful in assessing the distortion of the spectrum when the flat strips are replaced by corrugated ones. This is the topic of the next section.

3.1 | Spectrum distortion by sinusoidally corrugated strips: 'anti-symmetric' case

Parallel corrugated strips resonators with *symmetric* and *anti-symmetric* location of the strips (see Figure 1) should be analysed separately because their impact on the spectrum of complex relative wavenumbers is different, even with the same geometrical parameters of the corrugated strips. This is explained by different conditions in the formation of standing waves between the corrugated strips. For both planar and corrugated strips in an *anti-symmetric location*, the distance $D(x)$, $-L \le x \le L$, between corresponding points on two strips does not vary ($D(x) = d = const$); for a symmetric location of the plates, the distance varies according to $D(x) = d + 2h\sin(2\pi n_T x/L)$, $-L \le x \le L$.

On facing a multi-parameter problem, we are forced to restrict ourselves to such combinations of parameters which may highlight the basic regularities of the perturbation to the spectrum once corrugation is introduced. We set $d/2L = 0.5$ for all the calculations carried out in this section. In addition, we describe the corrugated strips by sinusoids $y(x) = \pm d + h\sin(2\pi\, n_T x/L)$, $-L \le x \le L$, where the number of periodic corrugations takes values $n_T = 4, 8, 16, 32$, and the relative corrugation depth takes the values $h/d = 0.01, 0.02, 0.05, 0.1$.

First, using the approach described in Section 2.2, we find the first three complex eigenvalues when $h/d = 0.01$ as the number of the periods varies over $n_T = 4, 8, 16, 32$. Depending upon the number of the periods $n_T = 4, 8, 16, 32$ the corrugation parameter h/T takes the values $h/T = 0.02, 0.04, 0.1, 0.2$. The investigated structures are shown in Figure 5. The results for $\gamma_{n,1}$ ($n = 1, 2, 3$) have been calculated with accuracy of five decimal digits and collected in Table 3. The real parts $\gamma'_{n,1}(n = 1, 2, 3)$ of the complex eigenvalues slowly increase with the growth of the number of the periods, n_T, which populate the strips of the same fixed length. This phenomenon is due to the contraction of the effective distance d_{eff} between the corrugated strips as n_T increases: the effective value of the aspect ratio $d/2L = 0.5$, which is characteristic for a parallel planar strips resonator, becomes slightly reduced to $d_{\text{eff}}/2L = 0.5 - \delta$, where $\delta = 1 - d_{\text{eff}}/d \ll 1$. The lowering of this aspect ratio should reduce the *radiation losses* from the resonator. This physically reasonable assumption is well supported by the data from Table 3 for the imaginary parts $\gamma''_{n,1}$ of the complex eigenvalues $\gamma_{n,1}(n = 1, 2, 3)$.

For corrugations of a small scale, we observe minor increases in the unloaded Q-factor: we may compare the values $Q_{1,1} = 12.1549$, $Q_{2,1} = 56.4622$, and $Q_{3,1} = 146.545$ for the parallel-strip resonator with non-corrugated strips with the values $Q_{1,1} = 12.3234$, $Q_{2,1} = 57.1089$, and $Q_{3,1} = 147.727$, calculated for the corrugated strips with parameters $h/d = 0.01$ and $n_T = 32$.

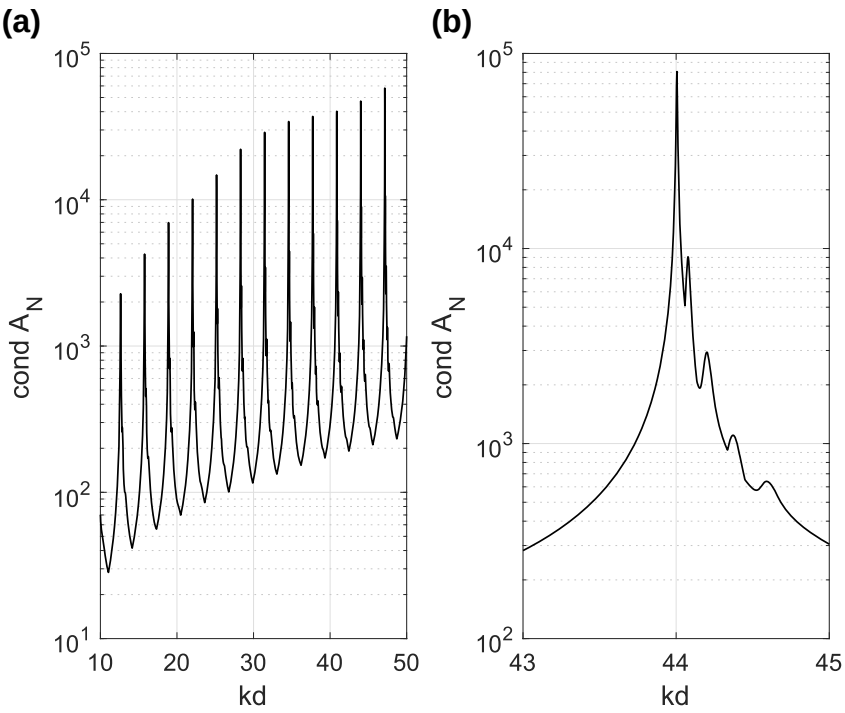

FIGURE 4 Dependence $cond(A_{N_{tr}})(kd)$ for parallel-strip resonator $(d/2L = 0.5)$: (a) in a wider interval of kd values; (b) magnified view of one of the parts $cond(A_{N_{tr}})(kd)$

TABLE 2 Complex eigenvalues $\gamma_{n,m}$ for higher oscillations $(n = 14)$ in parallel-strip resonator $(d/2L = 0.5)$

$\gamma_{n,m}$	$cond(A)$	**Formula (5)**	$\gamma_{n,m} = \gamma'_{n,m} - i\gamma''_{n,m}$	Q - factor, $Q_{n,m}$
$\gamma_{14,1}$	44.005	44.010	44.00683–i0.003401	$6.4688 \cdot 10^3$
$\gamma_{14,2}$	44.078	44.094	44.08024–i0.013877	$1.5881 \cdot 10^3$
$\gamma_{14,3}$	44.201	44.234	44.20260–i0.03064	$7.2126 \cdot 10^2$
$\gamma_{14,4}$	44.372	44.428	44.37407–i0.05583	$3.9735 \cdot 10^2$
$\gamma_{14,5}$	44.592	44.678	44.59151–i0.08728	$2.5544 \cdot 10^2$

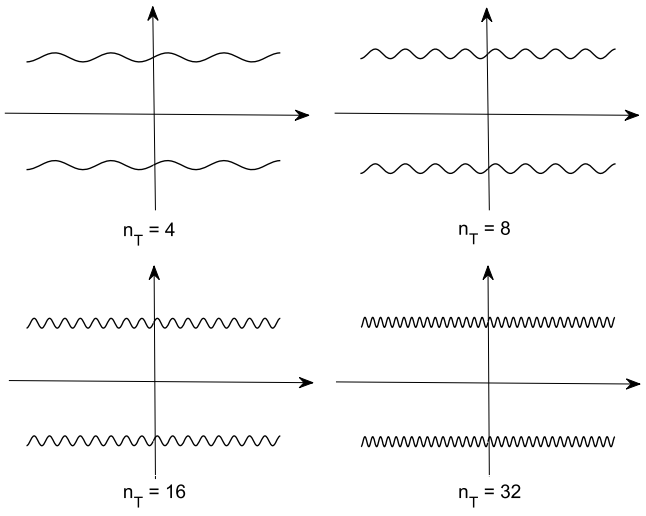

FIGURE 5 Visualization of the parallel-strip resonator $(d/2L = 0.5)$ with sinusoidally corrugated strips $(n_T = 4,\ 8,\ 16,\ 32)$

It has been found that the most crucial role in the distortion of the spectrum is played by the parameter h/d, that is, the depth of corrugation. The influence of the different depths of corrugation $(h/d = 0,\ 0.01,\ 0.02,\ 0.05,\ 0.1)$ on the spectrum of the first three complex oscillations, characterized by the complex eigenvalues $\gamma_{n,1}(n = 1,\ 2,\ 3)$, is shown in Table 4.

TABLE 3 Complex eigenvalues $\gamma_{n,m}$ of the resonator $(d/2L = 0.5)$ with sinusoidally corrugated $(h/d = 0.01,\ n_T = 4,\ 8,\ 16,\ 32)$ strips (anti-symmetric)

n_T	$\gamma_{1,1}$	$\gamma_{2,1}$	$\gamma_{3,1}$
4	3.33347–i0.13701	6.41629–i0.05682	9.52606–i0.03268
8	3.33732–i0.13692	6.42454–i0.05684	9.54000–i0.03260
16	3.34431–i0.13666	6.43899–i0.05676	9.56234–i0.03257
32	3.35519–i0.13613	6.46131–i0.05657	9.59636–i0.03248

In the case of fixed small depth $(h/d = 0.01)$, the reduction of the effective distance d_{eff} is achieved by an increase in the number of periods n_T. The contraction (in a physical sense) of the distance between plates is due to the growth of the corrugation depth. Whatever the reason, the contraction of the geometrical distance, d, to a smaller effective distance, d_{eff}, leads, as in the previous case, to a discernible positive shift in

the real parts $\gamma'_{n,1}(n = 1, 2, 3)$ of the complex eigenvalues $\gamma_{n,1}$ and reduction of their imaginary parts $\gamma''_{n,1}$. As observed before, this leads to an increase of the unloaded Q-factor, but now the scale of increase is significantly higher. In fact, let us compare the values of $Q = Q(h/d)$ as a function of the relative corrugation depth h/d: $Q_{1,1}(0) = 12.1549$ and $Q_{1,1}(0.1) = 16.0413$; $Q_{2,1}(0) = 56.4622$ and $Q_{2,1}(0.1) = 76.0074$; $Q_{3,1}(0) = 146.545$ and $Q_{3,1}(0) = 202.8703$.

Once the parameter h/d exceeds 0.1, there is a threshold at which the regular spectrum of the complex oscillations, characteristic for a parallel-strip resonator with non-corrugated strips, collapses. It is known that, in practice, the *suppression of higher modes* in waveguides (equally, in resonators) can be achieved by the corrugation of the waveguide walls. The collapse of the spectrum regularity, or equivalently, suppression of the higher modes, will occur when the depth of corrugation $2h$ becomes comparable at some frequency with wavelength λ: $2h \sim \lambda$. We verify this assertion by computation of $cond(A_{N_{tr}})(d/\lambda)$ in a wide frequency range for more extreme values of the corrugation parameter, taking $h/d = 0.1$, 0.2 and $h/d = 0.3$, 0.4. Corrugated strips with these parameters are illustrated in Figure 6 and the corresponding dependence $cond(A_{N_{tr}})(d/\lambda)$ in Figure 7.

The behaviour of the plots $cond(A_{N_{tr}})(d/\lambda)$ clearly reveals the progressive suppression of the higher modes as the depth of corrugation increases (from $h/d = 0.1$ to $h/d = 0.4$). The second phenomenon is *spectrum rarefaction* for the lowest complex oscillations (modes). In fact, if we restrict ourselves to the interval up to $d/\lambda \sim 4$, one can find seven oscillations with higher Q-factor when $h/d = 0.1$, five when $h/d = 0.2$, three when $h/d = 0.3$, and only one when $h/d = 0.4$. The mechanism leading to the suppression of higher modes and the apparent resonance 'chaos' at higher frequencies may be explained by the coupling of irregular modes which emerge due to the formation of standing waves between the tops of sinusoids, between the tops and bottoms, and so on. In principle, a description of this phenomenon might be given using the basic Geometric Optics (*GO*) postulates. It would be useful only when other arguments are exhausted which, in our case, is not so: the *MAR*-based algorithm obviates the need. One example supporting this assertion is of spectrum rarefaction for lower modes occurring at a pronounced corrugation depth where $h/d \geq 0.2$.

TABLE 4 Complex eigenvalues $\gamma_{n,m}$ in the resonator $(d/2L = 0.5)$ with sinusoidally corrugated $(h/d = 0,\ 0.01,\ 0.02,\ 0.05,\ 0.1,\ n_T = 16)$ strips (anti-symmetric)

h/d	$\gamma_{1,1}$	$\gamma_{2,1}$	$\gamma_{3,1}$
0	3.32976–i0.13697	6.40958–i0.05676	9.51839–i0.03247
0.01	3.34431–i0.13666	6.43899–i0.05676	9.56234–i0.03257
0.02	3.38134–i0.13588	6.51373–i0.05673	9.67421–i0.03274
0.05	3.55042–i0.13225	6.85399–i0.05577	10.18403–i0.03237
0.1	3.92627–i0.12238	7.60530–0.05003	11.30799–i0.02787

It should be stressed that the formation of the single mode regime in the resonator, with only $TM_{1,1}$ - mode, occurs when $h/d = 0.4$, the complex eigenvalue is $\gamma_{1,1} = 12.7177 - i0.01659$, and the unloaded Q-factor is $Q_{1,1} = 3.8329 \cdot 10^2$.

3.2 | Spectrum distortion by sinusoidally corrugated strips: 'symmetric' case

At small relative depths of corrugation $(h/d \ll 1)$, the character of spectrum distortion in open resonators with symmetric location of the corrugated strips has much in common with that obtained when the relative position of the strips is anti-symmetric (see Section 3.1). The situation changes at the moderate sizes of the parameter h/d and is completely different at high values of h/d, especially when this parameter approaches its maximum permissible value of 0.5 (see Figure 1b). In these cases, we are really dealing with a multi-chamber open resonator or a waveguide bounded by sinusoidal walls. It is this case that we study in this section.

The problem geometry is shown in Figure 8. The bounding curve, matching the resonator walls, is described by a function of form $y(x) = \pm d/2 + h\cos mx$. In our calculations, we use parameters $m = 2\pi$, $d = 1$ and the relative size of the entry slot $w_d = 1 - 2\frac{h}{d}$, where $\frac{h}{d} < 0.5$. Since $d = 1$, then parameters w and w_d coincide numerically, and because $m = 2\pi$, the period $T = 1$. Of course, the choice of parameters for this multi-parameter problem is not unique. Nevertheless, studies of the spectrum with these chosen parameters reflect all the basic and principal peculiarities characteristic for this class of structures. For definiteness, we choose the geometry of a unit chamber (or cell) described by the parameter $d/2L = 1$.

The first step is to examine the complex eigenvalues for a single cell, as shown in Figure 8a. Then we study the spectrum of complex eigenvalues for the multi-chamber structure when

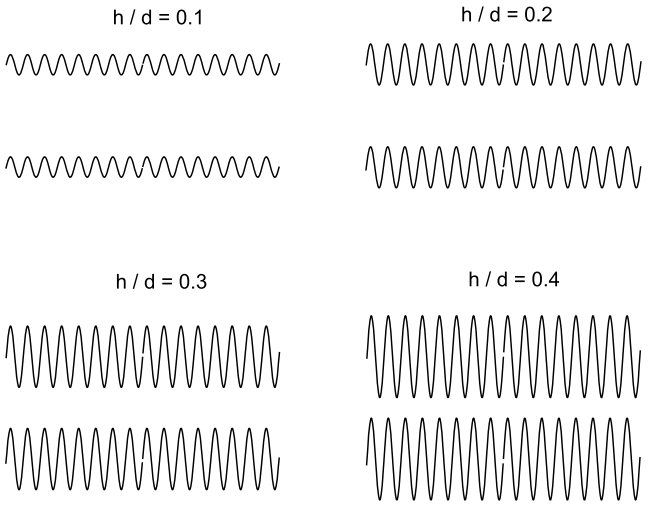

FIGURE 6 Visualization of the parallel-strip resonators $(d/2L = 0.5,\ n_T = 16)$ with increasing deeply corrugated anti-symmetric strips: $h/d = 0.1,\ 0.2,\ 0.3,\ 0.4$

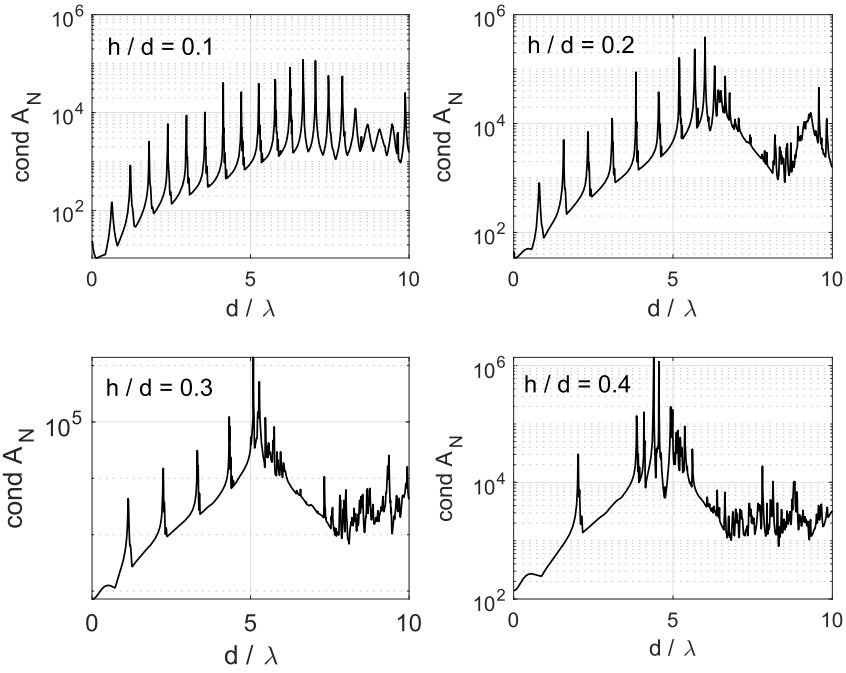

FIGURE 7 Condition number $cond(A_{N_{tr}})$ versus wave size of distance, d/λ with parameters $d/2L = 0.5$ and $h/d = 0.1,\ 0.2,\ 0.3,\ 0.4$

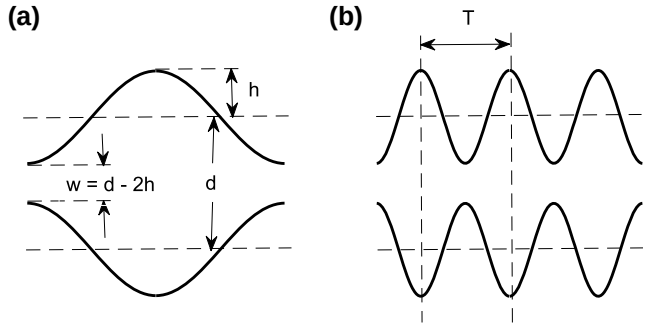

FIGURE 8 Multi-chamber resonator: (a) unit cell ($n_T = 1$); (b) several cells ($n_T > 1$)

$n_T = 3$ and $n_T = 7$. An open resonator of such shape may equally be regarded as a chain of coupled resonators. Though, it deserves a more complete investigation, we carried out studies primarily to find certain properties of the spectrum and restricted ourselves to examination of the first two complex oscillations. Treating the value kd as a spectral parameter, we examined the interval $3 \le kd \le 7.5$, where, according to the preliminary calculations of $cond(A_{N_{tr}})(kd)$, the first two complex eigenvalues lie. Since, there is no obvious specification of these oscillations in the domains which are bounded by non-canonical curves, we introduce the notations $\chi_n^{(n_T)}, n = 1, 2; n_T = 1, 3, 7$ for the complex eigenvalues. As shown before, calculation of the frequency dependence $cond(A_{N_{tr}})(kd)$ gives a detailed picture of the spectrum composition in the chosen frequency range. We used three values of the parameter w_d–0.6, 0.4 and 0.2–to examine slots that are relatively wide, moderate or narrow, respectively. The results of the calculations are shown in Figures 9–11, where dependence $cond(A_{N_{tr}})(kd)$ is shown in different parts of the diapason on kd.

The analysis of dependence $cond(A_{N_{tr}})(kd)$ leads us to make the following conclusions: First and foremost, the functions $cond(A_{N_{tr}})(kd)$ clearly reveal all the fine details which occur in the process of electromagnetic coupling between the individual waveguide sections. In addition, the physically reasonable assumption about the slot width w_d as a measure of coupling is confirmed: the wider the slot width w_d, the stronger the electromagnetic coupling. It can be seen from the plots that the resonance frequencies split in the transition from the single-cell resonator to its multi-cell configuration. This phenomenon has much in common with the occurrence of a spectral line as a multiplet. For certain parameters (for a slot wide enough and an appropriate ordinal number of the complex mode) the frequency splitting is governed by a simple rule: the resultant number of split frequencies coincides exactly with the number of cells in the multi-cell resonator. The exception to this rule occurs only in the case when the complex oscillation possesses a very high value of the unloaded Q-factor for a single-section resonator $(n_T = 1)$. The weak coupling is enough to make the resonance frequency shift but is not sufficient to produce a frequency split. Such a situation is shown in Figure 11 $(w_d = 0.1)$ for an oscillation with the complex eigenvalue $\chi_2^{(n_T)}, n_T = 1, 3, 7$. Such behaviour is explained by the extraordinarily high Q-factor: $Q_2^{(1)} = 5.2621 \cdot 10^{10}$. This data is extracted from Table 5, in which we collected the complex eigenvalues $\chi_n^{(1)}(n = 1, 2)$, calculated for a single-section resonator with relative slot widths $w_d = 0.6,\ 0.4,\ 0.1$. The accuracy of calculations is not lower than 5 decimal digits.

The distinctive behaviour of a frequency septet in the case of a moderately sized slot $(w_d = 0.4)$ is shown in Table 6. In presenting the cut-off relative wave numbers in this table, we use the notation $\chi_{n(s)}^{(n_T)}$, where along with the previously used notations (with values $n = 1,\ 2$ and $n_T = 1,\ 3,\ 7$) we introduce the new parameter s taking values $s = 1, 2, \ldots, n_T$, standing for the serial

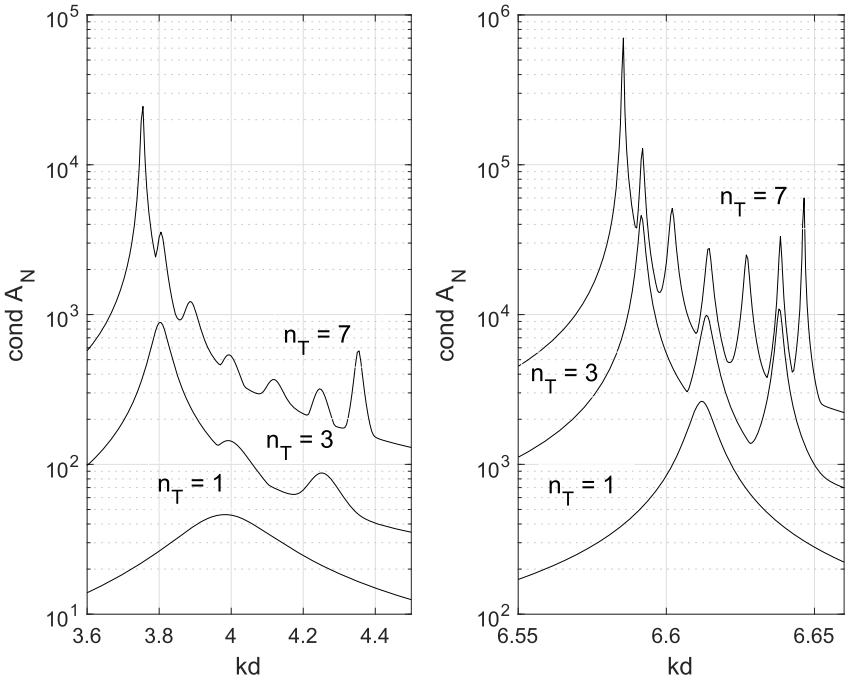

FIGURE 9 Frequency dependence $cond(A_{N_T})(kd)$ for a single-cell $(n_T = 1)$ and multi-cell $(n_T = 3, 7)$ resonator $(d/2L = 1, w_d = 0.6)$

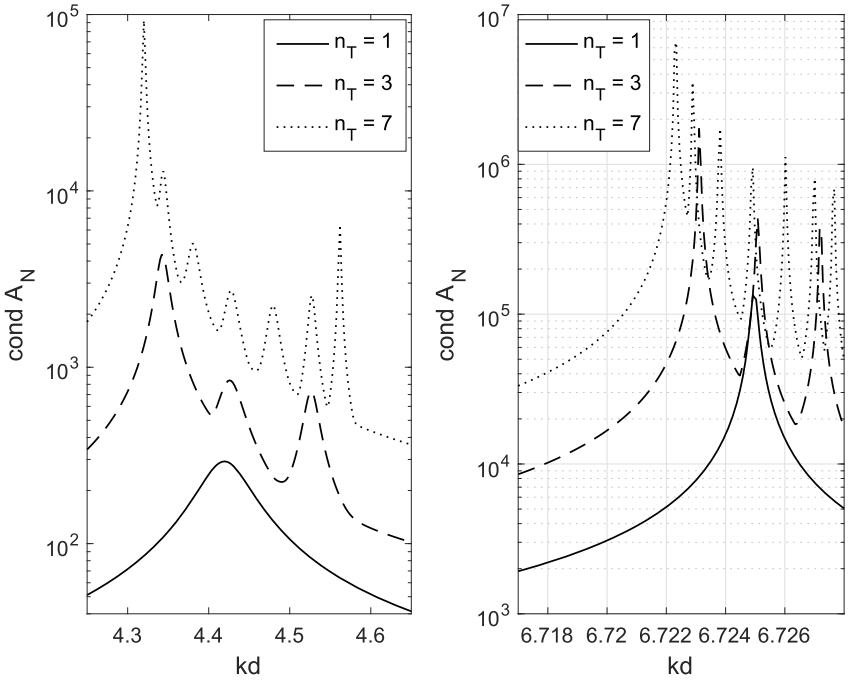

FIGURE 10 Frequency dependence $cond(A_{N_T})(kd)$ for a single-cell $(n_T = 1)$ and a multi-cell $(n_T = 3, 7)$ resonator $(d/2L = 1, w_d = 0.4)$

number of the split wave numbers $\chi^{(n_T)}_{n(s)}$, which are arranged in an ascending order of value. The nature of the septet structure is now explained using the data for this septet $\chi^{(7)}_{2(s)}$, $s = 1, 2, \ldots, 7$ (see the last column in Table 6). The central position in this septet (of index $s = 4$) has the value $\chi^{(7)}_{2(4)} = 6.72517 - i2.616 \cdot 10^{-5}$. Comparison of this value with that of the eigenvalue of the second complex mode in the single-cell resonator, $\chi^{(1)}_2 = 6.72496 - \mathrm{i}0.000104$ (see Table 5), shows that $Re(\chi^{(7)}_{2(4)})$ is closer to $Re(\chi^{(1)}_2)$ among all the other values $Re(\chi^{(7)}_{2(s)}), s \neq 4$. In addition, the value of the corresponding Q-factor, $Q^{(7)}_{2(4)} = -Re(\chi^{(7)}_{2(4)})/(2Im(\chi^{(7)}_{2(4)})) = 1.2854 \cdot 10^5$, is the lowest in the septet. At the same time, the Q-factors with the lowest index $(s = 1)$ and the highest index $(s = 7)$, namely $Q^{(7)}_{2(1)} = 7.5029 \cdot 10^5$ and $Q^{(7)}_{2(7)} = 9.7789 \cdot 10^5$, are maximal amongst the Q-factors in the septet. Roughly speaking, the distribution of the values $Q^{(7)}_{2(s)}$ is nearly symmetrical, relative to the minimal central value $Q^{(7)}_{2(4)}$. This case is entirely typical in reflecting the general features of the frequency-splitting phenomenon in multi-cell symmetric resonators with deeply corrugated strips.

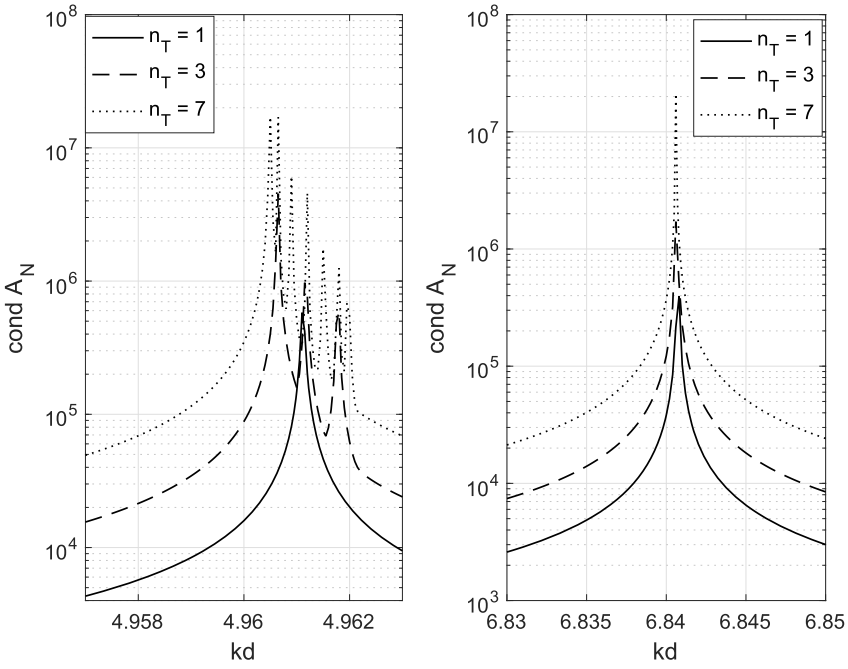

FIGURE 11 Frequency dependence $cond(A_{N_{tr}})(kd)$ for a single-cell $(n_T = 1)$ and a multi-cell $(n_T = 3,\ 7)$ resonator $(d/2L = 1, w_d = 0.1)$

TABLE 5 Cut-off wave numbers $\chi_n^{(1)}, n = 1, 2$ and quality factors $Q_n^{(1)}$ in a single-cell resonator

w_d	$\chi_1^{(1)}$	$Q_1^{(1)}$	$\chi_2^{(1)}$	$Q_2^{(1)}$
0.6	3.97785–i0.13127	$1.5151 \cdot 10^{1}$	6.61197–i0.00404	$8.1831 \cdot 10^{2}$
0.4	4.41945–i0.03038	$7.2736 \cdot 10^{1}$	6.72496–i0.000104	$3.2332 \cdot 10^{4}$
0.1	4.96113–i0.000024	$1.0336 \cdot 10^{5}$	6.84073–i6.5·10^−11	$5.2621 \cdot 10^{10}$

TABLE 6 Complex eigenvalues $\chi_n^{(7)}, n = 1, 2$ and quality factors $Q_n^{(7)}$ in a multi-cell resonator $(w_d = 0.4)$

$cond(A_{N_{tr}})$	$\chi_1^{(7)}$	$cond(A_{N_{tr}})$	$\chi_2^{(7)}$
4.320	$\chi_{1(1)}^{(7)} = 4.32061$–i0.00105	6.7225	$\chi_{2(1)}^{(7)} = 6.72257$-i4.48·10^−6
4.344	$\chi_{1(2)}^{(7)} = 4.34472$–i0.00365	6.7231	$\chi_{2(2)}^{(7)} = 6.72317$–i1.432·10^−5
4.380	$\chi_{1(3)}^{(7)} = 4.38234$–i0.00638	6.7240	$\chi_{2(3)}^{(7)} = 6.72408$–i2.403·10^−5
4.428	$\chi_{1(4)}^{(7)} = 4.42969$–i0.00771	6.7251	$\chi_{2(4)}^{(7)} = 6.72517$–i2.616·10^−5
4.480	$\chi_{1(5)}^{(7)} = 4.48103$–i0.00683	6.7262	$\chi_{2(5)}^{(7)} = 6.72629$–i2.133·10^−5
4.528	$\chi_{1(6)}^{(7)} = 4.52842$–i0.00416	6.7272	$\chi_{2(6)}^{(7)} = 6.72725$–i1.204·10^−5
4.562	$\chi_{1(7)}^{(7)} = 4.56244$–i0.00126	6.7279	$\chi_{2(7)}^{(7)} = 6.72791$–i3.44·10^−6

4 | SCATTERING OF AN OBLIQUELY INCIDENT E-POLARIZED PLANE WAVE BY A PARALLEL CORRUGATED STRIP RESONATOR

The accurate determination of the complex eigenvalues $\gamma_{n,1}$ (anti-symmetric strip location) in Section 3.1 makes the resonance response from a parallel sinusoidally corrugated strips resonator a predictable phenomenon. For its study, we apply an *external excitation*, which is an oblique incident E-polarized plane wave (see Figure 1). The near field of the resonator may be described by calculation of its surface current density (*SCD*), or more exactly the jump in *SCD* across the surface of each strip. Let $J_{upp}(\theta)$ and $J_{low}(\theta)$ denote the jump in SCD for the upper and lower plates, respectively, where θ is the parameterization angle $(-\pi \le \theta \le \pi)$.

For computation, we use the data contained in the previously constructed Table 1 (planar strips resonator), Table 3 (parallel corrugated strips (anti-symmetric) resonator) and Table 7. In Table 7, we present the data for a parallel corrugated strips (anti-symmetric) resonator with aspect ratio $d/2L = 0.1$ and parameters: $n_T = 4,\ 16; h/d = 0,\ 0.025,\ 0.05,\ 0.1$. In contrast to the case where $d/2L = 0.5$, the phenomenon of resonance excitation for case $d/2L = 0.1$ is much more pronounced. This

contrast is explained by the very substantially higher values of the Q-factors for the same complex modes which exist, as in the resonator with parameter $d/2L = 0.5$ than that with parameter $d/2L = 0.1$. For example, with parameters $n_T = 16$ and $h = h/d = 0.1$, the $TM_{11} - mode$ has a complex eigenvalue $\gamma_{1,1} = 3.92627 - i0.12238$ with $Q_{1,1} = 16.0413$ when $d/2L = 0.5$, whereas $\gamma_{1,1} = 3.424294 - i0.0020772$ with $Q_{1,1} = 824.2572$ when $d/2L = 0.1$.

It should be observed that under *external excitation* the incidence angle α plays a role similar to that of the location of a long electric dipole providing *internal excitation*. In the first case, effective excitation of a certain $TM_{n,m}$-mode depends strongly on the interval in which the incidence angle α varies. When excitation is supplied by a long electric dipole (a mathematical model of the waveguide post used in radio-engineering), optimal excitation occurs when the post is placed at the maximum *EM* field intensity of some concrete mode which is targeted for excitation. As an example of such a procedure, we demonstrate the excitation of the parallel-strip resonator with non-corrugated plates. For the sake of clarity, we use the parameters $d/2L = 0.5$ and $h/d = 0$. Excitation of the complex TM_{21} - mode occurs when $kd = Re(\gamma_{2,1})$, where $\gamma_{2,1} = 6.409589 - i0.056760$ ($Q_{2,1} = 56.4622$). The results of the calculations are presented in Figure 12.

Because the magnitude of the Q-factor is low (56.4622), the complete TM_{21} - mode cannot be effectively excited. Under such circumstances, by varying the incidence angle α, one can find an interval of α in which the currents $\lfloor J_{low}(\theta) \rfloor$, $\lfloor J_{upp}(\theta) \rfloor$ start to reveal, in their main features, a similarity with the ideal current distribution which is only realizable at extremely high magnitudes of the Q-factors. In our case this occurs in the interval $55^\circ \le \alpha \le 60^\circ$, where one can find the features of the oscillation belonging to the TM_{21} - mode: one variation (one maximum point) of the field occurs across each strip, and the maxima of both functions $\lfloor J_{low}(\theta) \rfloor$ and $\lfloor J_{upp}(\theta) \rfloor$ occur approximately at the middle of the strips. The sharp peaks at the edges of both strips arise due to the *edge effect*. We study the influence of corrugation on the behaviour of the currents $\lfloor J_{low}(\theta) \rfloor$ and $\lfloor J_{upp}(\theta) \rfloor$, using results for current resonances in the parallel-strip resonator with non-corrugated strips when the incidence angle $\alpha = 57^\circ$. Despite some peculiarities in the distribution of the currents across the lower ($J_{low}(\theta)$) and upper ($J_{upp}(\theta)$) strips shown in Figure 12, we concentrate on the

TABLE 7 Complex eigenvalues $\gamma_{n,1}, n = 1, 2$ in the resonator ($d/2L = 0.1$, $n_T = 4, 16$) with corrugated strips ($h/d = 0,\ 0.025,\ 0.05,\ 0.1$), antisymmetric location

Complex eigenvalues (relative wave numbers, $\gamma_{n,1}$)			
$\gamma_{n,1}$	h	$n_T = 4$	$n_T = 16$
$\gamma_{1,1}$	0	**3.155724–i0.002224**	**3.155724–i0.002224**
	0.025	3.158387–i0.002225	3.174235–0.0022155
	0.05	3.166358–i0.002231	3.227959–i0.002189
	0.1	3.197985–i0.00225166	3.424294–i0.0020772
$\gamma_{2,1}$	0	**6.290506–i0.000711**	**6.290506–i0.000711**
	0.025	6.29656–i0.0007223	6.32093–i0.0007087
	0.05	6.31459–i0.0007565	6.40895–0.0007143
	0.1	6.38444–i0.00086779	6.72418–i0.0006590
$\gamma_{3,1}$	0	**9.42972–i0.0003678**	**9.42972–i0.0003678**
	0.025	9.43890–i0.0003770	9.45092–i0.0003763
	0.05	9.46593–i0.0004588	9.50944–i0.00021355
	0.1	9.56856–i0.0052883	9.68658–i0.00001602

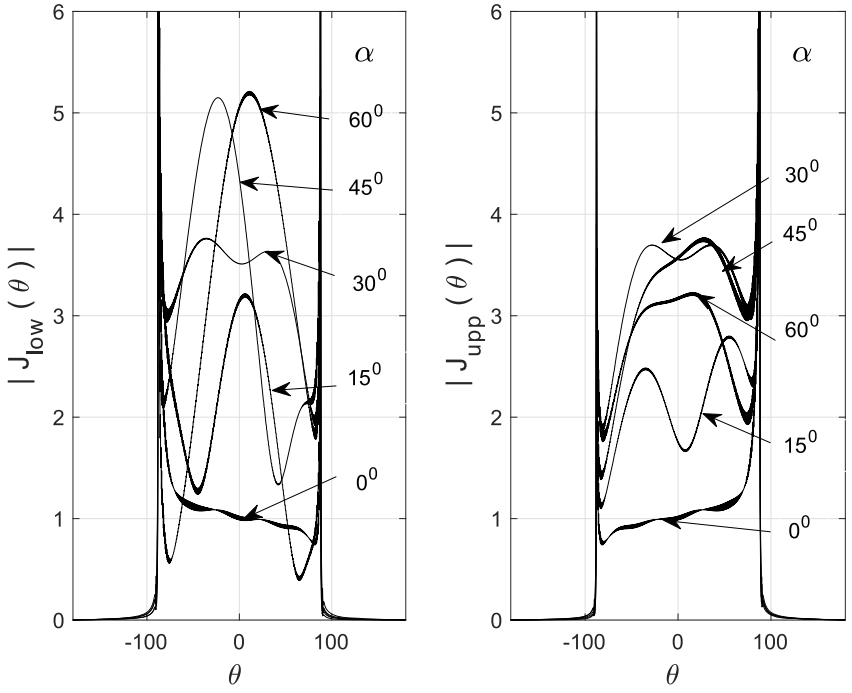

FIGURE 12 Distribution of the SCD's $J_{low}(\theta)$and $J_{upp}(\theta)$ across the lower and upper non-corrugated strips, respectively, at the resonant relative wave number $kd = Re(\gamma_{2,1}) = 6.409589$; $d/2L = 0.5$; $h/d = 0$

calculation of $J_{\text{low}}(\theta)$, since these peculiarities are not of principal character and only emerge at low values of Q_{n1}.

The first group of calculations address the degree of influence of the corrugation depth h/d on the reference distribution $J_{\text{low}}^{\text{ref}}(\theta)$ of the non-corrugated lower strip (Figure 12). The deviation of the currents $J_{\text{low}}(\theta)$ as the corrugation depth h/d grows is shown in Figure 13. The calculations used the same parameters as in Table 4: $d/2L = 0.5$, $n_T = 16$ and $h/d = 0,\ 0.01,\ 0.02,\ 0.05,\ 0.1$. In the second group of calculations we fix a low-profile corrugation ($h/d = 0.01$) and increase the number of periods ($n_T = 4,\ 8,\ 16,\ 32$), leaving the plate width $2L$ constant. These calculations use the data shown in Table 3; the results are displayed in Figure 14.

In both cases, resonance scattering occurs when $kd = Re(\gamma_{21})$. In the first case (shown in Figure 13), the wave size of each strip $2L/\lambda$ varies from $2L/\lambda = 2.0402$ ($h/d = 0$) to $2L/\lambda = 2.4208$ ($h/d = 0.1$). The wave size of each period T/λ varies from $T/\lambda = 0.1275$ to $T/\lambda = 0.1513$, respectively.

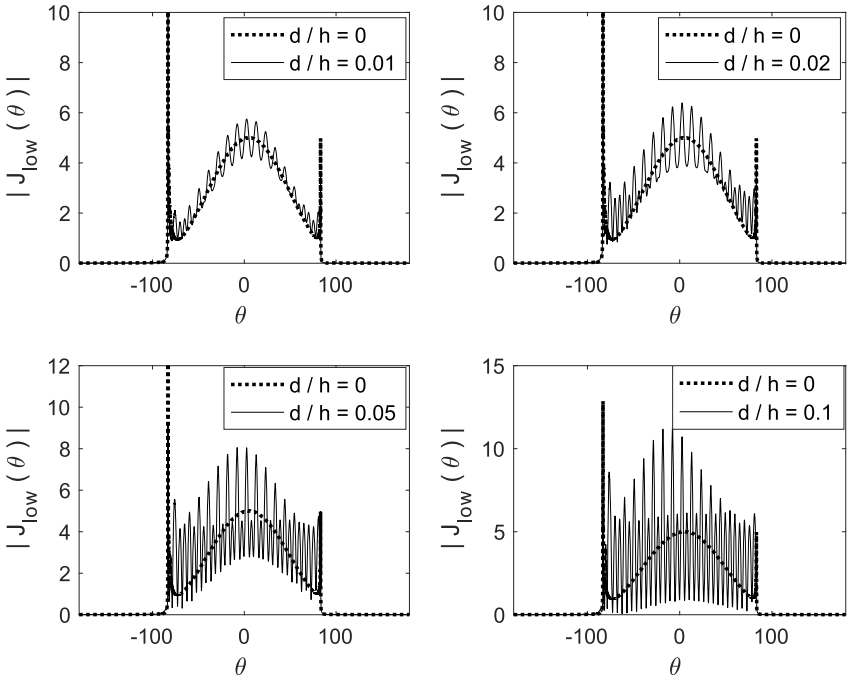

FIGURE 13 Influence of the sinusoidal corrugation on resonance current distribution $J_{\text{low}}(\theta)$: $d/2L = 0.5,\ n_T = 16,\ h/d = 0,\ 0.01,\ 0.02,\ 0.05,\ 0.1;\ kd = Re(\gamma_{21})$

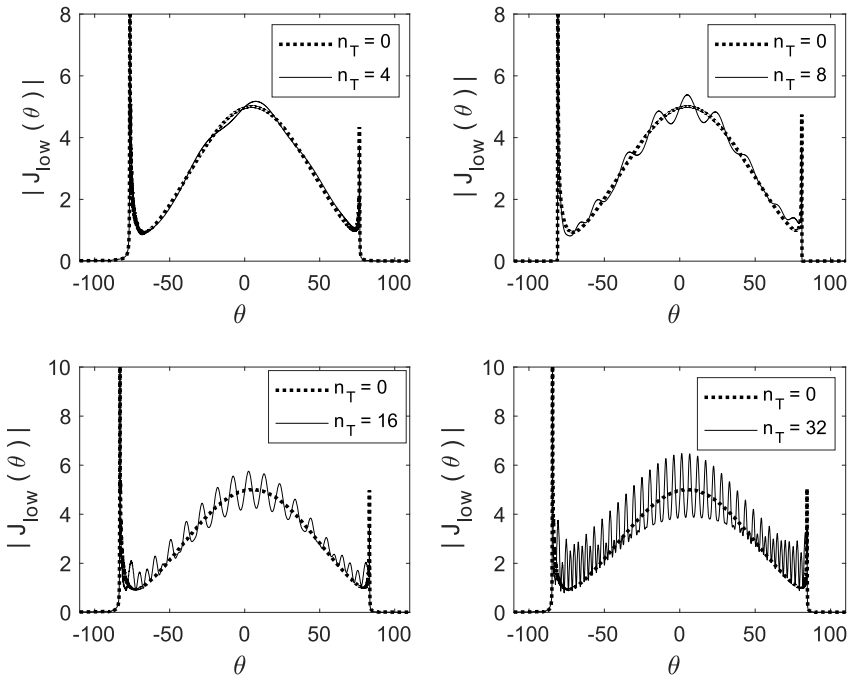

FIGURE 14 Influence of the sinusoidal corrugation on resonance current distribution $J_{\text{low}}(\theta)$: $d/2L = 0.5,\ h/d = 0.01,\ n_T = 4,\ 8,\ 16,\ 32,\ kd = Re(\gamma_{21})$

This allows us to treat the local *EMF* in the neighbourhood of the sinusoidal peaks as quasi-static fields; this explains the appearance of the current spikes at the peaks. This phenomenon strengthens with the growth of the corrugation depth when the aspect ratio h/T (depth relative to sinusoid period) varies from $h/T = 0$ $(h/d = 0)$ to $h/T = 1.6$ $(h/d = 0.1)$.

The same mechanism explains the behaviour of the SCD $J_{\text{low}}(\theta)$ presented in Figure 14. When the corrugation factor is small $(h/d = 0.01)$ and the number of periods is small $(n_T = 4,\ T/\lambda \sim 0.5)$, there is minimal distortion in the reference distribution $J^{\text{ref}}_{\text{low}}(\theta)$ (see Figure 14a). Successive increments of the number of periods $(n_T = 8,\ 16,\ 32)$ lead to the sharpening of the sinusoidal peaks. Also, due to the diminishing aspect ratio $(T/\lambda \sim 0.25, 0.125,\ 0.063)$, the local *EMF* in the close vicinity of the peaks becomes quasi-static so that the linear waist of the peak is less compared to the wavelength. In this case the peaks are "sensed" by the quasi-static *EMF* as sharp edges. As a consequence, the current distribution $J_{\text{low}}(\theta)$ at the sinusoidal peaks has sharp spikes, the amplitude of which increases as the number of periods grows $(n_T = 8,\ 16,\ 32)$.

The distinction between the excitation of the parallel-strip resonator with sinusoidally corrugated strips at the resonance $(kd = Re(\gamma_{21}))$ and at the slightly shifted frequencies $kd = Re(\gamma_{21}) \mp \delta$ is shown in Figure 15. By considering the well-known definition of the *Q*-factor $(Q = f_r/\Delta f$, where f_r is the resonant frequency and Δf the full width at half-maximum (FWHM)), the following condition for δ was used:

$$\lfloor \delta \rfloor \geq Re(\gamma_{n1})/Q_{n1} \text{ or } \lfloor \delta \rfloor \geq 2 \lfloor Im(\gamma_{n1}) \rfloor > 0.$$

For example, for the TM_{21} - mode in the resonator with the parameters used in Figures 13–15(see Table 4), among the five values of corrugation depth considered, the maximum value of $Im(\gamma_{21})$ occurs when the parameter $h/d = 0$; in this case $Im(\gamma_{21}) = 0.05676$. Hence, the condition becomes $\delta \geq 0.11352$. For calculations, we use $\delta = 0.15$.

It is of interest to compare the resonance currents for the parallel-strip resonator with the parameters investigated in Figures 13–15 and to contrast the cases when the TM_{nm} - modes have low and high *Q*-factors. The growth of the *Q*-factor directly depends on the reduction of the aspect ratio $d/2L$. A concrete case with a smaller aspect ratio $d/2L = 0.1$ is tabulated in Table 7; we extract those data which concern the complex eigenvalues attributed to the TM_{n1} - mode $(n = 1,\ 2,\ 3)$. The calculations reveal that optimal excitation of the TM_{n1} - modes by a plane wave, when resonance currents reach their maxima, occurs at a differing range of incident angles, depending on the number n of standing waves between strips. For this reason, we examine the following modes at the indicate angle α of incidence: $TM_{11}(\alpha = 15^\circ)$; $TM_{21}(\alpha = 40^\circ)$; and $TM_{31}(\alpha = 50^\circ)$. The calculations of the SCD $J(\theta)$ are presented in Figure 16.

In general, the behaviour of the SCD $J_{\text{low}}(\theta)$ for both the cases $d/2L = 0.5$ (Figure 13) and $d/2L = 0.1$ (Figure 16) is similar, except that the amplitude of oscillations $J_{\text{low}}(\theta)$ is much lower for the latter case. This is no surprise because the wave size $2L/\lambda$ is five times larger, and although the number of the periods is the same for both cases $(n_T = 16)$, the ratio T/λ is also five times larger. Whilst for the case $d/2L = 0.5$ the peaks of the sinusoids were operating in quasi-static *EMF*, in the case $d/2L = 0.1$ they lie in the diffraction frequency region $(T \sim \lambda)$, roughly, $T/\lambda \approx 0.31$ (TM_{11}), $T/\lambda \approx 0.62$ (TM_{21}), and $T/\lambda \approx 0.94$ (TM_{31}). In such circumstances, the peaks of sinusoids cannot be treated (in an electromagnetic sense) as sharpened parts of the plates. This weakens the edge effect and hence lowers the amplitude of $\lfloor J_{\text{low}}(\theta) \rfloor$.

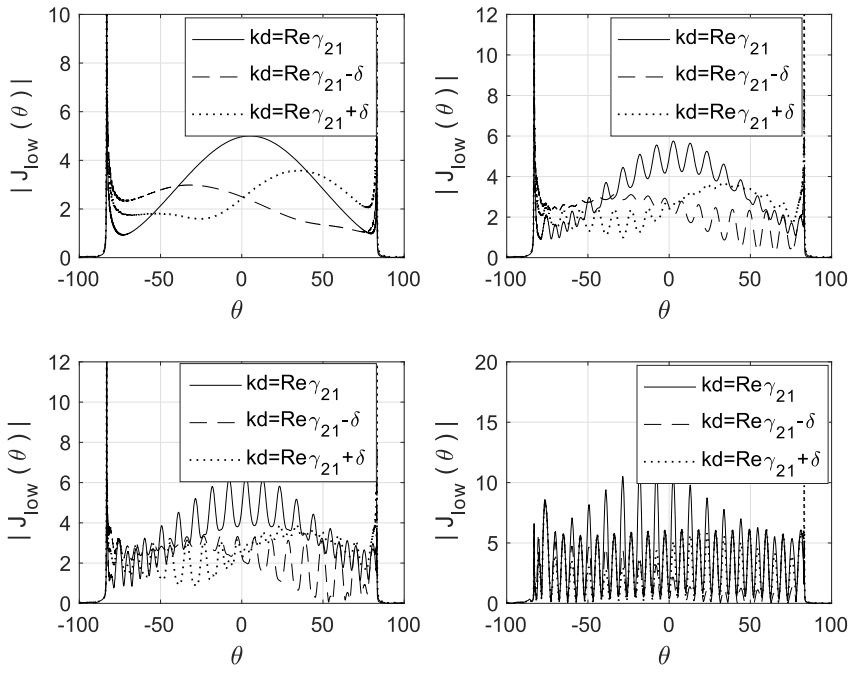

FIGURE 15 Excitation of the TM_{21} - mode at non-resonant frequencies for the parallel-strip resonator with the par $kd = Re\gamma_{21} \mp \delta$ in a resonator with differing depths of corrugation $h/d = 0,\ 0.01,\ 0.02,\ 0.1$ and at an angle of incidence $\alpha = 57^\circ$ $(d/2L = 0.5,\ n_T = 16)$

So far, we have focused on the dominant modes TM_{n1}, characterized by only one EMF variation across the horizontal direction ($m = 1$). Without investigating the case $m > 1$ in full, it should be noticed such TM_{nm} - modes are excited more efficiently than the TM_{n1} - modes. As an example, Figure 17 shows the distribution $J_{\text{low}}(\theta)$ arising when the TM_{32} - mode is excited in a corrugated resonator with the parameters $d/2L = 0.1$, $n_T = 16$, and $h/d = 0.1$. In this case, $\gamma_{32} = 9.68923 - \text{i}0.000044$, whereas the corresponding non-corrugated parallel-strip resonator has $\gamma_{32}^{(0)} = 9.44455 - \text{i}0.001472$. The angle of incidence inducing near optimal response is $\alpha = 45^\circ$. The much-diminished responses at slight shifts $\delta = \pm 0.001$ from the resonant frequency are also shown.

5 | CONCLUSIONS

The controllable high accuracy of the Method of Analytical Regularization has been used for investigation of the spectrum of structures comprising two perfectly conducting surface-relief gratings of finite size with sinusoidal corrugation. For

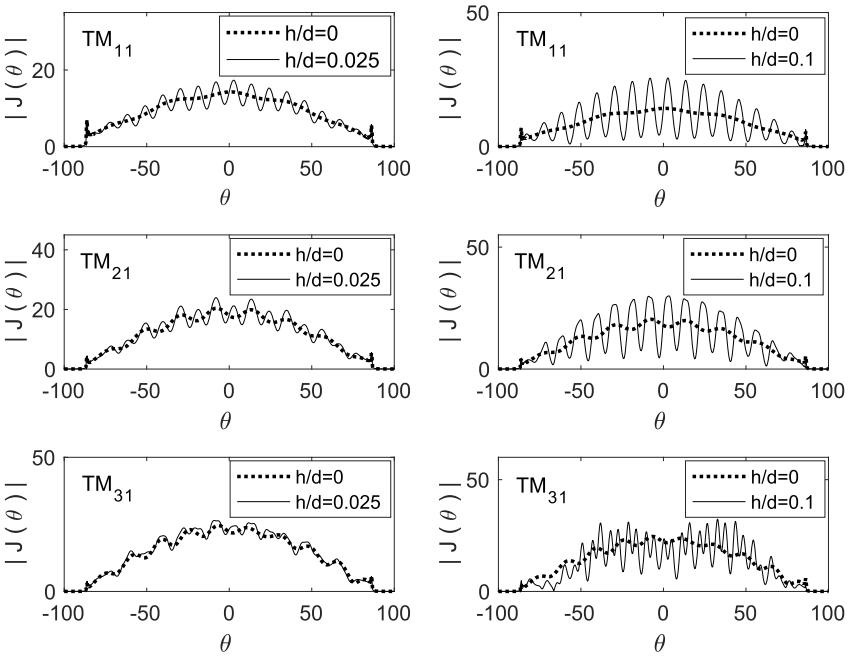

FIGURE 16 Influence of the sinusoidal corrugation on resonance current distribution $J_{\text{low}}(\theta)$: $d/2L = 0.1$, $h/d = 0.025,\ 0.01$, $n_T = 8$, $kd = Re(\gamma_{n1})$ (Table 7): $\alpha = 15^\circ$ (TM_{11}), $\alpha = 40^\circ$ (TM_{21}), and $\alpha = 50^\circ$ (TM_{31})

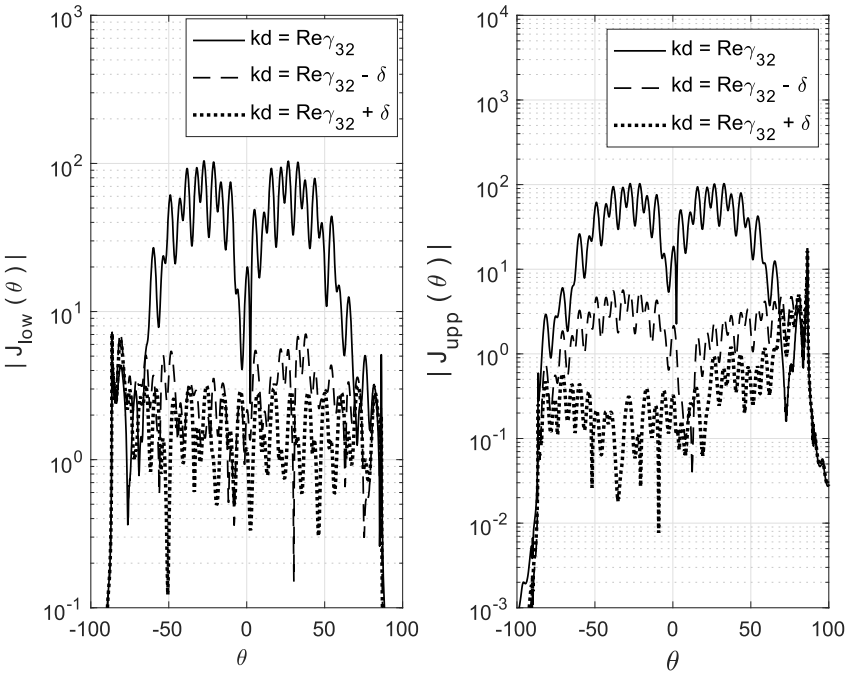

FIGURE 17 SCDs for the TM_{32} - mode in a corrugated resonator with the parameters $d/2L = 0.1$, $n_T = 16$, and $h/d = 0.1$. It is excited by a field incident at angle $\alpha = 45^\circ$. The frequency shift parameter is $\delta = 0.001$

comparison purposes, we also carried out an analogous investigation of the parallel-strip resonators.

The focus of investigation targeted the calculation of the complex eigenvalues, corresponding to complex $TM_{n,m}$ modes, as a necessary prerequisite for the examination of resonance scattering of such structures by an obliquely incident E-polarized plane wave. The high-accuracy calculation of the complex eigenvalues allowed us to obtain reliable results on excitation of selected $TM_{n,m}$ modes; precise identification of the modes extracted from the spectrum has been realized through examination of the calculated surface current density jump at the surface of each sinusoidally corrugated strip in the resonant regime of excitation.

In the calculations, two types of resonators were used. One is a resonator formed by parallel translation of one of the sinusoidally corrugated strips and the second is obtained by rotation of one of the strips in the first type of resonator.

Further studies of this and related problems will naturally investigate complex oscillations of transverse electric type ($TE_{n,m}$). Although the change of polarization induces some significant changes to the method, the *MAR* can be appropriately adapted and effectively used to solve such problems.

Another fascinating direction is the study of so-called 'lattice modes (LM)' arising in periodically corrugated Fabry–Perot resonators. They are absent if the PEC strips are flat but become manifest with high (or ultra-high) Q-factors provided the number of periods is 'large' (say 10-20-50) and the depth of the grooves is 'small', smaller than the period. At normal incidence, the frequency of the lowest LM occurs when the ratio of the period to the wavelength is $1-\delta$, where the parameter $\delta \ll 1$ depends on the groove depth and shape. A review of this phenomenon is given in [21]. Although the parameter ranges fall outside those studied in the present article, its methods are obviously adaptable for such a future study.

ORCID

Elena D. Vinogradova https://orcid.org/0000-0003-2817-0741

REFERENCES

1. Gaylor, T.K., Moharam, M.G.: Analysis and applications of optical diffraction by gratings. Proc. IEEE. 73(5), 894–937 (1985)
2. Bonod, N., Neauport, J.: Diffraction gratings: from principles to applications in high-intensity lasers. Adv. Opt. Photon. 8(1), 156–199 (2016)
3. Palmer, C.: Diffraction Grating Handbook, 6th ed. Newport Corporation (2005)
4. Popov, E.: Introduction to diffraction gratings: summary of applications. In: Popov, E. (ed) Gratings: Theory and Numeric Applications, Chapter 1. Institut Fresnel, CNRS, AMU (2012)
5. Zaginaylov, G.I., Rozhkov, A.A., Raguin, J.-Y.: Theory of beam-plasma instability in a periodic plasma-filled waveguide. Phys. Rev. E. 60(6), 7391–7399 (1999)
6. Zaginaylov, G.I., Gandel, Y.V., Turbin, P.V.: Modeling of plasma effect on the diffraction radiation of relativistic beam moving over a grating of finite extent. Microwave Opt. Technol. Lett. 16(1), 50–54 (1997)
7. Borzenkov, A.V., Sologub, V.G.: Scattering of a plane wave by two strip resonators. Radio Eng. Electron. Phys. 20(5), 30–38 (1975)
8. Kaliberda, M.E., Lytvynenko, L.M., Pogarsky, S.A.: Operator method in the analysis of electromagnetic wave diffraction by planar screens. J. Commun. Technol. Electron. 54, 975–981 (2009). https://doi.org/10.1134/S1064226909090010
9. Kaliberda, M.E., et al.: Diffraction of the H-polarized plane wave by a finite layered graphene strip grating. Int. J. Microw. Wirel. Technol. 11(4), 326-333 (2019). https://doi.org/10.1017/S1759078718001290
10. Mata-Mendez, O., Chavez-Rivas, F.: Diffraction of Gaussian and Hermite–Gaussian beams by finite gratings. J. Opt. Soc. Am. A. 18(3), 537–545 (2001)
11. Sumaya-Martinez, J., Mata-Mendez, O., Chavez-Rivas, F.: Rigorous theory of the diffraction of Gaussian beams by finite gratings: TE polarization. J. Opt. Soc. Am. A. 20(5), 827–835 (2003)
12. Cwik, T., Mittra, R.: The effects of the truncation and curvature of periodic surfaces: a strip grating. IEEE Trans. Antennas Propag. 36, 612–622 (1988)
13. Tsitsas, N.L., Mittra, R.: Analysis of truncated gratings and a novel technique for extrapolating their characteristics to those of infinite gratings. Appl. Comput. Electromagn. Soc. J. 32(6), 463–472 (2017)
14. Kalhor, H.A.: Plane metallic gratings of finite numbers of strips. IEEE Trans. Antennas Propag. 37(3), 406–407 (1989)
15. Vinogradova, E.D., Kobayashi, K., Eizawa, T.: Full wave analysis of plane wave diffraction by a finite sinusoidal grating: E-polarization case. Wave Motion. 86, 44–62 (2019). https://doi.org/10.1016/j.wavemoti.2018.12.006
16. Eizawa, T., Kobayashi, K.: Wiener–Hopf analysis of the H-polarized plane wave diffraction by a finite sinusoidal grating. Prog. Electromagn. Res. 149, 1–13 (2014)
17. Eizawa, T., Kobayashi, K.: Plane wave diffraction by a finite parallel-plate waveguide with sinusoidal wall corrugation. Prog. Electromagn. Res. B. 73, 61–78 (2017)
18. Vinogradova, E.D.: Complex eigenvalues of slotted arbitrary cylindrical cavities: sound-soft elliptic cavity with variably placed longitudinal slit. J. Acoust. Soc. Am. 144, 1146 (2018). https://doi.org/10.11231/1.5052693
19. Vinogradova, E.: Electromagnetic plane wave scattering by arbitrary two-dimensional cavities: rigorous approach. Wave Motion. 70, 47–64 (2017). https://doi.org/10.1016/j.wavemoti.2016.06.009
20. Vinogradov, S.S., Smith, P.D., Vinogradova, E.D.: Canonical Problems in Scattering and Potential Theory. Part 1: Canonical Structures in Potential Theory. Chapman & Hall/CRC, Boca Raton, FL (2001)
21. Byelobrov, V.O., et al.: Periodicity Matters: grating or lattice resonances in the scattering by sparse arrays of subwavelength strips and wires. IEEE Antennas Propag Mag. 57(6), 34–45 (2015). https://doi.org/10.1109/MAP.2015.2480083

How to cite this article: Vinogradova, E.D., Kobayashi, K.: Complex eigenvalues of natural *TM*-oscillations in an open resonator formed by two sinusoidally corrugated metallic strips. IET Microw. Antennas Propag. 15(10), 1283–1298 (2021). https://doi.org/10.1049/mia2.12166